Article

Cell Reports

Porcupine Controls Hippocampal AMPAR Levels, Composition, and Synaptic Transmission

Graphical Abstract

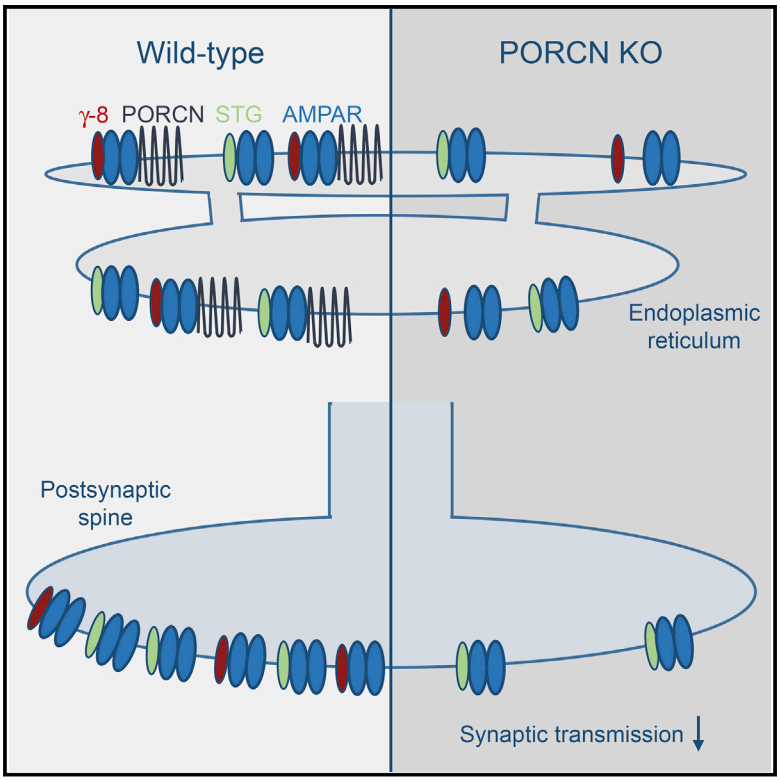

Authors

Nadine Erlenhardt, Hong Yu, Kavitha Abiraman, Tokiwa Yamasaki, Jacques I. Wadiche, Susumu Tomita, David S. Bredt

Correspondence

dbredt@its.jnj.com

In Brief

Recent proteomic studies have identified an array of proteins associated with AMPA-type glutamate receptors. Erlenhardt et al. now systematically survey this collection, finding that the membrane-bound O-acyl transferase PORCN plays a crucial role in regulating basal synaptic transmission by controlling AMPAR complex composition and stability at the level of the ER.

Highlights

- PORCN controls assembly and stability of hippocampal AMPARs at the level of the ER
- PORCN knockout reduces basal synaptic transmission but not long-term potentiation
- Functional interaction with AMPARs is independent of PORCN's catalytic activity

Erlenhardt et al., 2016, Cell Reports *14*, 1–13
February 2, 2016
http://dx.doi.org/10.1016/j.celrep.2015.12.078

CellPress

Please cite this article in press as: Erlenhardt et al., Porcupine Controls Hippocampal AMPAR Levels, Composition, and Synaptic Transmission, Cell Reports (2016), http://dx.doi.org/10.1016/j.celrep.2015.12.078

Cell Reports
Article

Porcupine Controls Hippocampal AMPAR Levels, Composition, and Synaptic Transmission

Nadine Erlenhardt,[1,2,5] Hong Yu,[1,5] Kavitha Abiraman,[3,5] Tokiwa Yamasaki,[4] Jacques I. Wadiche,[3] Susumu Tomita,[4] and David S. Bredt[1,*]

[1]Neuroscience Discovery, Janssen Pharmaceutical Companies of Johnson & Johnson, 3210 Merryfield Row, San Diego, CA 92121, USA
[2]Institute of Neural and Sensory Physiology, Medical Faculty, University of Düsseldorf, 40225 Düsseldorf, Germany
[3]Department of Neurobiology, McKnight Brain Institute, University of Alabama at Birmingham, Birmingham, AL 35294, USA
[4]CNNR program, Department of Cellular and Molecular Physiology, Yale University School of Medicine, 295 Congress Avenue BCMM441, P.O. Box 208026, New Haven, CT 06510, USA
[5]Co-first author
*Correspondence: dbredt@its.jnj.com
http://dx.doi.org/10.1016/j.celrep.2015.12.078

SUMMARY

AMPA receptor (AMPAR) complexes contain auxiliary subunits that modulate receptor trafficking and gating. In addition to the transmembrane AMPAR regulatory proteins (TARPs) and cornichons (CNIH-2/3), recent proteomic studies identified a diverse array of additional AMPAR-associated transmembrane and secreted partners. We systematically surveyed these and found that PORCN and ABHD6 increase GluA1 levels in transfected cells. Knockdown of PORCN in rat hippocampal neurons, which express it in high amounts, selectively reduces levels of all tested AMPAR complex components. Regulation of AMPARs is independent of PORCN's membrane-associated O-acyl transferase activity. PORCN knockdown in hippocampal neurons decreases AMPAR currents and accelerates desensitization and leads to depletion of TARP γ-8 from AMPAR complexes. Conditional PORCN knockout mice also exhibit specific changes in AMPAR expression and gating that reduce basal synaptic transmission but leave long-term potentiation intact. These studies define additional roles for PORCN in controlling synaptic transmission by regulating the level and composition of hippocampal AMPAR complexes.

INTRODUCTION

AMPA-type glutamate receptors underlie most excitatory synaptic transmission in brain. In addition to mediating moment-to-moment signaling, AMPARs undergo activity-dependent functional changes, which mediate aspects of the synaptic plasticity that underlies learning and memory (Anggono and Huganir, 2012; Ehlers, 2000; Huganir and Nicoll, 2013; Malinow and Malenka, 2002; Nicoll et al., 2006; Sheng and Kim, 2002). Molecular manifestations of this plasticity include changes in AMPAR protein synthesis, post-translational modification, channel trafficking, and subunit composition.

Assembly of neuronal AMPAR complexes is precisely controlled. AMPARs comprise heterotetramers of the glutamate-binding, pore-forming subunits GluA1–4 (Boulter et al., 1990; Seeburg, 1993). Distinct combinations of GluA subunits and their alternative splicing and post-transcriptional editing impart differential physiological properties to AMPARs (Boulter et al., 1990; Seeburg, 1993). Additionally, AMPAR complexes often contain multiple classes of auxiliary subunits (Kato et al., 2010; Yan and Tomita, 2012). The auxiliary subunit composition and stoichiometry of AMPARs varies, even within a single neuronal type, and this imparts differential properties at specific synaptic types (Coombs and Cull-Candy, 2009; Jackson and Nicoll, 2011). Furthermore, the molecular composition of neuronal AMPARs dynamically changes as part of synaptic plasticity (Bats et al., 2013; Jackson and Nicoll, 2011). Molecular mechanisms that control assembly of AMPARs remain poorly understood.

The first identified auxiliary subunit, stargazin, is essential for AMPAR function in cerebellar granule neurons (Hashimoto et al., 1999). Subsequently, a family of six transmembrane AMPAR regulatory proteins (TARPs) were defined that modify channel trafficking, gating, and pharmacology (Kato and Bredt, 2007; Tomita et al., 2003). Cornichons (CNIH-2/3) are a family of AMPAR auxiliary subunits that control export of AMPARs from the endoplasmic reticulum (Harmel et al., 2012; Schwenk et al., 2009) and associate with synaptic AMPARs to modulate channel kinetics (Jackson and Nicoll, 2011; Kato et al., 2010; Schwenk et al., 2009; Yan and Tomita, 2012). Recent proteomic studies have further expanded the complement of AMPAR-associated proteins. The cysteine-knot protein CKAMP44 modulates AMPAR biophysics to attenuate short-term synaptic plasticity in the dentate gyrus (von Engelhardt et al., 2010). The germ cell-specific gene 1-like (GSG1-l) modifies gating and kinetics of receptor channels in a subunit-dependent manner (Schwenk et al., 2012; Shanks et al., 2012). Furthermore, more than two dozen proteins occur in AMPAR complexes (Schwenk et al., 2012). These additional AMPAR partners include integral transmembrane, extracellular GPI-anchored, and secreted proteins.

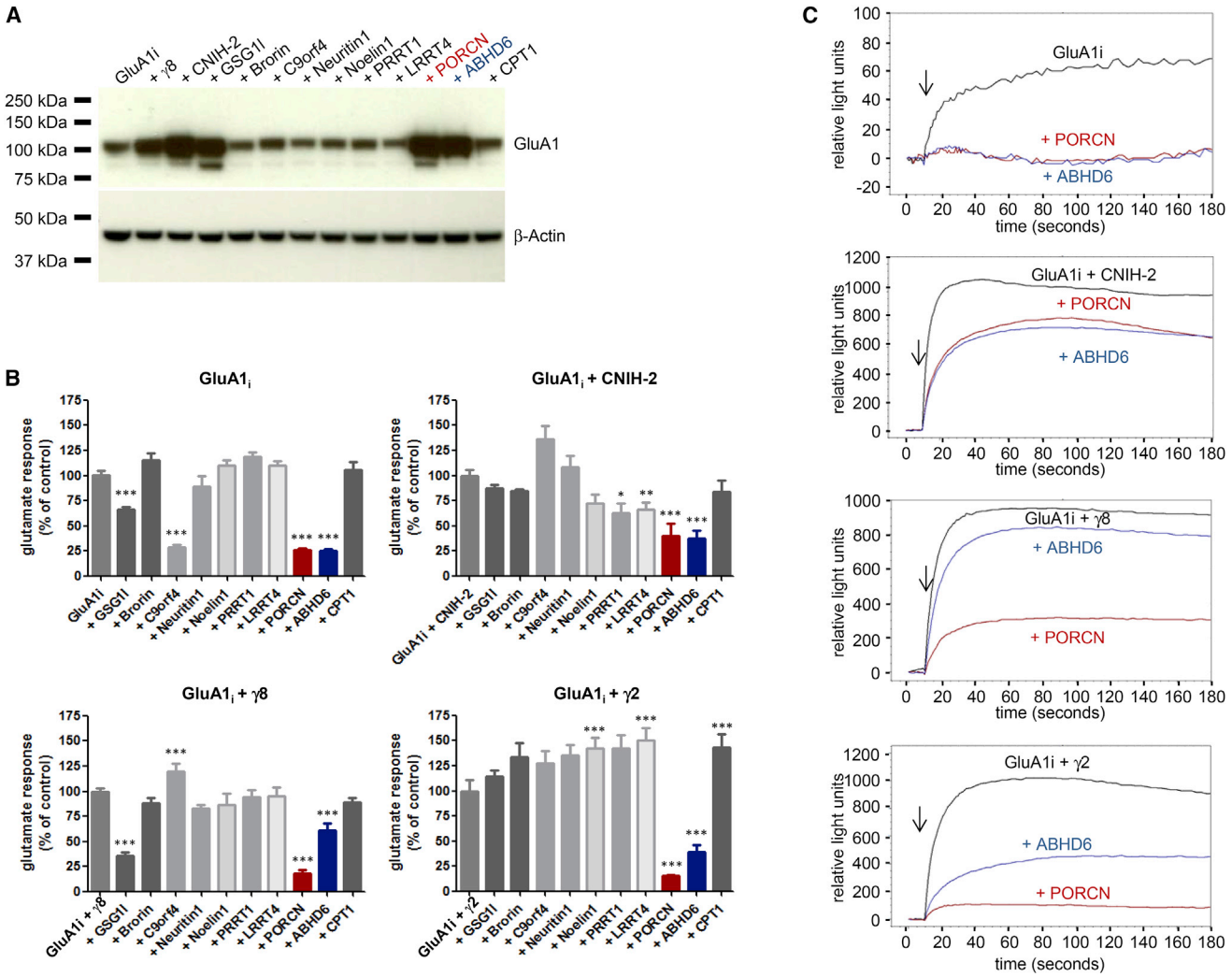

Figure 1. PORCN and ABHD6 Change GluA1 Expression and Steady-State Currents

(A) Immunoblotting of whole-cell lysates from HEK293T cells transfected with cDNAs encoding GluA1i alone or together with the cDNA indicated. β-actin serves as loading control. In addition to previously characterized γ-8, CNIH-2, and GSG1l, only PORCN and ABHD6 increase GluA1 levels.

(B) Quantification of glutamate-evoked calcium influx measured by FLIPR in HEK293T cells transfected with GluA1 alone or GluA1 + γ-8 or γ-2. Only PORCN (red) and ABHD6 (blue) consistently affect the responses evoked by 100 μM glutamate. Data are shown as mean + SEM, n = 8–12. *p < 0.05, **p < 0.01, ***p < 0.001.

(C) Representative FLIPR traces. Arrows indicate the addition of 100 μM glutamate.

Some partners have enzymatic activities; some are cytoskeletal elements; and others are secreted growth factor antagonists. Understanding how this large and diverse protein collection modulates AMPARs is an important challenge.

Here, we find that previously well-characterized AMPAR auxiliary subunits TARP, CNIH-2, and GSG1-l dramatically increase GluA1 protein levels in heterologous cells. By systematically evaluating each class of protein found in AMPAR immunoprecipitates (Schwenk et al., 2012), we demonstrate that porcupine (PORCN) and ABHD6 also increase levels of co-transfected GluA1. We find that PORCN controls hippocampal AMPARs, as PORCN knockdown destabilizes AMPAR complexes and thereby diminishes synaptic transmission. AMPAR complexes in PORCN-deficient neurons have deficient TARP γ-8 and show accelerated decay kinetics. This work defines functional roles for AMPAR partners in controlling stability and composition of receptor complexes.

RESULTS

GluA1 Protein Levels Controlled by Transmembrane AMPAR-Associated Proteins

TARP γ-8 knockout diminishes AMPAR protein levels in neurons (Rouach et al., 2005), and we found co-expression of γ-8 or CNIH-2 dramatically increases GluA1 levels in heterologous HEK293T cells (Figure 1A). We asked whether this increase in GluA1 occurs with other components identified in AMPAR immunoprecipitates. Accordingly, HEK cells were co-transfected with GluA1 and a representative from each protein family identified in neuronal AMPAR immunoprecipitates. Strikingly, we found that

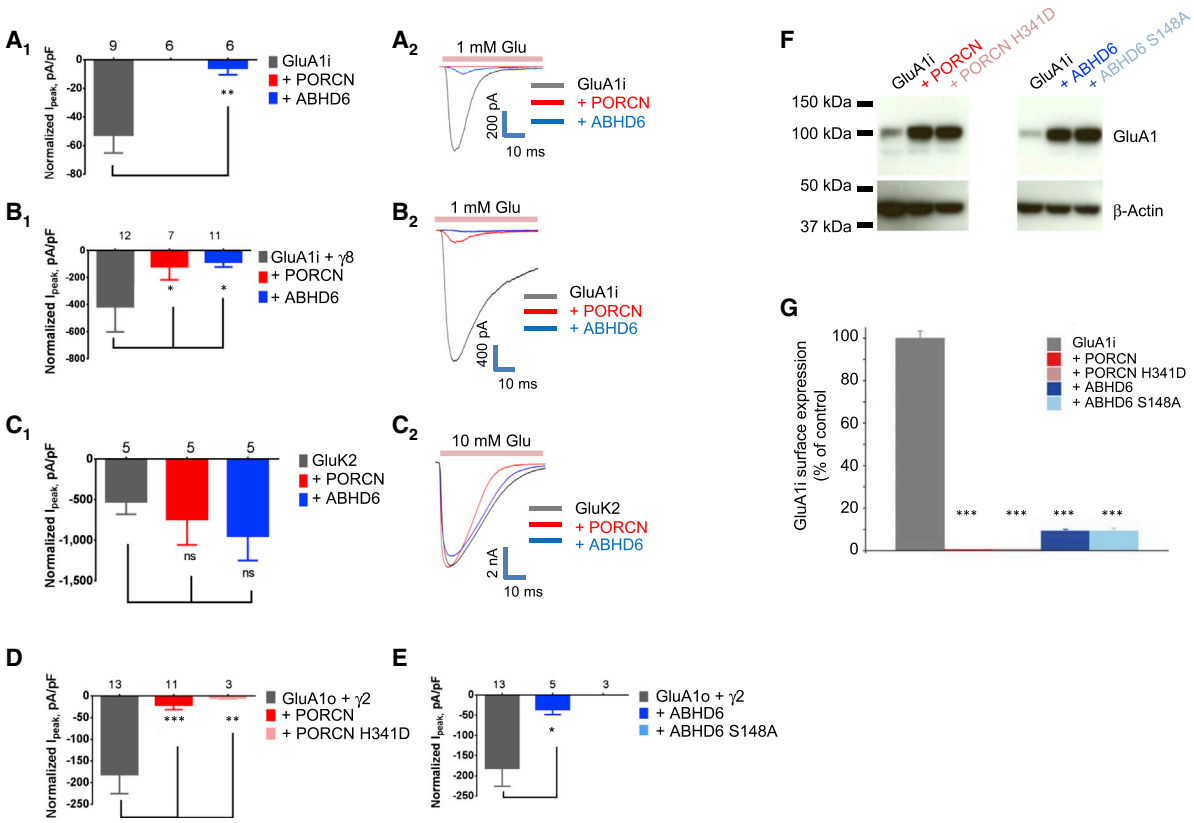

Figure 2. PORCN and ABHD6 Reduce Glutamate-Evoked Currents and Surface GluA1 Levels

(A–E) Glutamate-evoked currents in whole-cell recordings from HEK293T cells transfected with (A) GluA1i ± PORCN or ABHD6; (B) GluA1i + γ-8 ± PORCN or ABHD6; (C) GluK2 ± PORCN or ABHD6; (D) GluA1o + γ-2 ± PORCN or PORCN H341D; and (E) GluA1o + γ-2 ± ABHD6 or ABHD6 S148A. The subscripts 1 and 2 show (1) calculated data and (2) representative traces. PORCN and ABHD6 reduce glutamate-evoked currents from AMPAR (with or without TARP, A and B), but not from kainate receptors (C). Enzyme activity is not necessary for the observed effects of PORCN (D) or ABHD6 (E) on AMPAR currents.

(F) Whole-cell lysates of HEK293T cells expressing GluA1i alone or together with PORCN, PORCN H341D, ABHD6, or ABHD6 S148A. β-actin serves as loading control.

(G) Quantification of $GluA1_i$ surface expression by a chemiluminescence assay using an anti-HA antibody. Extracellularly HA-tagged GluA1 flip was expressed either alone or together with PORCN, PORCN H341D, ABHD6, or ABHD6 S148A. PORCN and ABHD6 WT as well as their mutants without enzymatic activity all significantly reduced $GluA1_i$ surface expression.

Data are shown as mean + SEM, n = 5. ***p < 0.001 compared to control. See also Figures S1 and S3.

GSG1-l, PORCN, and ABHD6 but not seven other AMPAR-associated proteins increased GluA1 levels (Figure 1A). These GluA1 increases were specific as β-actin levels were unchanged.

PORCN and ABHD6 Diminish AMPAR Steady-State Currents in Heterologous Cells

We next used a fluorescent imaging plate reader (FLIPR) assay to rapidly and systematically assess functional effects of AMPAR interacting proteins. This system (Molecular Devices) uses a calcium-sensitive dye to quantify glutamate-evoked gating of AMPARs transfected in HEK293T cells. In cells transfected with GluA1 flip splice variant (GluA1i), glutamate evokes a sustained increase in calcium influx, and this is significantly reduced by GSG1-l, PORCN, ABHD6, or C9orf4 (Figures 1B and 1C). Additional series of GluA1i co-transfections with γ-2 or γ-8 showed that only PORCN and ABHD6 reduced glutamate-evoked gating in AMPARs containing these auxiliary subunits (Figures 1B and 1C).

PORCN and ABHD6 Restrict AMPAR Surface Trafficking in Heterologous Cells

Next, we evaluated functional effects of PORCN and ABHD6 by recording glutamate-evoked whole-cell currents in co-transfected HEK cells. Whereas PORCN and ABHD6 *increased* total AMPAR levels in these cells, glutamate-evoked whole-cell currents were dramatically *reduced* (Figure 2A). In HEK cells co-transfected with ABHD6, AMPAR-mediated currents were decreased by ~90%, and essentially no currents could be detected in cells co-transfected with PORCN (Figure 2A).

Next, we asked whether these effects of PORCN and ABHD6 could be reversed by TARPs. As previously reported, γ-8 and γ-2 increased glutamate-evoked currents from GluA1 (cf. gray bar in Figure 2A with Figures 2B1, 2D, and 2E). We found that both PORCN and to a lesser extent ABHD6 reduced glutamate-evoked currents in cells containing γ-8 or γ-2 (Figures 2B, 2D, and 2E) or in cells containing γ-8 and γ-2 (determined by FLIPR assay, data not shown). GluA2 was affected by PORCN

Please cite this article in press as: Erlenhardt et al., Porcupine Controls Hippocampal AMPAR Levels, Composition, and Synaptic Transmission, Cell Reports (2016), http://dx.doi.org/10.1016/j.celrep.2015.12.078

and ABHD6 co-expression similarly as GluA1 (data not shown). These actions of PORCN and ABHD6 on AMPARs are specific, as they have no effect on glutamate-evoked currents from cells co-transfected with a kainate receptor (Figure 2C).

PORCN is a membrane-bound O-acyl transferase (MBOAT), which mediates palmitoylation of Wg/WNT proteins within the endoplasmic reticulum (ER) (Kadowaki et al., 1996; Lum and Clevers, 2012). ABHD6 is an α-β-hydrolase domain-containing postsynaptic protein, which controls the accumulation and efficacy of 2-arachidonoylglycerol (2-AG) at cannabinoid receptors (Marrs et al., 2010). Therefore, we asked whether enzymatic activities of PORCN and ABHD6 mediate their effects on AMPARs. Previous mutagenesis studies defined critical residues in PORCN (Covey et al., 2012) and ABHD6 (Navia-Paldanius et al., 2012) essential for enzymatic activity. Specifically, histidine 341 occurs in the active site of PORCN, and mutation of this residue to aspartic acid abolishes palmitoyl-transferase activity (Galli et al., 2007). Analogously, serine 148 is critical for hydrolase activity of ABHD6. We found that neither mutating the critical histidine in PORCN nor mutating the critical serine in ABHD6 blunts their effects on GluA1 (Figures 2D–2F). Furthermore, treating cells with the highly potent and specific PORCN inhibitor, Wnt-C59 (Proffitt et al., 2013), did not prevent the PORCN-mediated effects on GluA1 (Figure S3). These results indicate that PORCN and ABHD6 regulation of AMPARs does not involve their catalytic activities.

Because PORCN and ABHD6 increase total GluA1 protein levels and decrease channel function, we asked whether they control receptor surface expression. We quantified GluA1 surface levels using an extracellular tagging approach (Harmel et al., 2012). Strikingly, we found that co-transfection of GluA1 with either PORCN or ABHD6 reduces surface GluA1 by more than 99% or 90%, respectively (Figure 2G). Enzymatic activity of neither PORCN nor ABHD6 are necessary for the reduction of GluA1 surface levels (Figure 2G).

We also assessed the effect of PORCN in oocytes, which lack AMPAR components and have been widely used to study effects of auxiliary subunits on channel trafficking and gating (Tomita et al., 2005). Oocytes were injected with cRNA encoding hemagglutinin-tagged GluA1 (HA-GluA1) alone or together with PORCN or the kainate receptor auxiliary subunit Neto2 (Straub and Tomita, 2012). As previously reported (Zhang et al., 2009), Neto2 had no significant effect on GluA1 currents or surface trafficking (Figure S1A). By contrast, PORCN abolished glutamate-evoked currents and dramatically reduced GluA1 surface levels (Figure S1C). This effect of PORCN is specific, as it had no effect on glutamate-evoked currents from oocytes injected with NMDA receptor subunits (Figure S1B).

Next, we asked whether the effect of PORCN in oocytes could be reversed by TARP γ-8. For these experiments, oocytes were injected with only 0.1 ng HA-GluA1 cRNA. Using this paradigm, γ-8 dramatically increases both HA-GluA1-mediated currents and HA-GluA1 surface expression (Figure S1D) (Tomita et al., 2005). In the presence of γ-8, PORCN suppresses both gating and surface trafficking of HA-GluA1 (Figures S1D and S1E). All of these effects are specific, as Neto2 does not affect GluA1 gating or trafficking (Figures S1D and S1E).

Overexpression of PORCN or ABHD6 Does Not Affect AMPAR Currents in Neurons

In situ hybridization shows that PORCN and ABHD6 are uniquely enriched in hippocampus (Lein et al., 2007). We therefore assessed effects of PORCN or ABHD6 in hippocampal neurons. We prepared hippocampal neurons from E18 Sprague Dawley rats, transfected them after 6–8 days in vitro, and recorded glutamate-evoked currents 14 days after transfection. We found that neither overexpression of PORCN nor overexpression of ABHD6 affected isolated AMPAR-mediated whole-cell currents (Figures 3A and 3B). Also, neither PORCN nor ABHD6 affected isolated NMDAR-mediated whole-cell currents. These experiments indicate that increasing PORCN or ABHD6 levels in hippocampal neurons does not affect AMPAR-mediated currents, which is likely explained by endogenous saturating amounts of PORCN and ABHD6.

PORCN Knockdown Selectively Blunts Neuronal AMPAR Currents and Accelerates Desensitization

To assess potential functions for endogenous PORCN and ABHD6, we employed short hairpin RNAs (shRNAs). We tested several possible sequences (data not shown) and arrived upon effective knockdown shRNAs for both PORCN and ABHD6. Six days following infection of hippocampal neurons with lentivirus expressing these shRNAs, we purified mRNA and performed qPCR. These experiments showed that the PORCN and ABHD6 shRNA selectively reduced their respective mRNAs without affecting β-actin or other mRNAs analyzed (Figure S2).

Next, we performed whole-cell recordings and measured glutamate-evoked currents in neurons co-transfected with GFP or with GFP plus shRNAs. We found that ABHD6 knockdown had no significant effects on AMPAR-mediated currents (Figures 3A and 3B). By contrast, PORCN knockdown dramatically reduced AMPAR-mediated currents (Figures 3A and 3B). When normalized to NMDA receptor-mediated currents on the same neurons, PORCN knockdown reduced AMPAR-mediated currents by >50%. Treating control neuronal cultures with the PORCN inhibitor Wnt-C59 did not change AMPAR/NMDA ratio, indicating that the effect on AMPAR-mediated currents was independent of PORCN activity (Figure S3B). In addition to reducing specifically the magnitude of AMPAR-mediated currents (Figure 3B), PORCN knockdown significantly accelerated channel desensitization (Figures 3C and 3D). This effect on AMPAR kinetics was specific, as NMDA receptor gating was unaffected (Figure 3E). As TARPs dramatically increase the ratio of kainate- to glutamate-evoked currents (Shi et al., 2009; Tomita et al., 2007), we quantified this ratio. In PORCN knockdown neurons, the kainate/glutamate ratio was unchanged (Figure 3F), suggesting the continued presence of a TARP. The acceleration of AMPAR kinetics is consistent with an exchange of γ-8 to γ-2 with PORCN knockdown, as γ-8 more profoundly slows desensitization (Cho et al., 2007; Milstein et al., 2007). As neither AMPAR kinetics (data not shown) nor AMPAR current amplitudes were changed by modulation of ABHD6 expression in hippocampal neurons, we focused on the PORCN-mediated effects on AMPARs in the rest of the study.

Next, we assessed effects of PORCN knockdown on synaptic AMPARs. In agreement with the effects on whole-cell

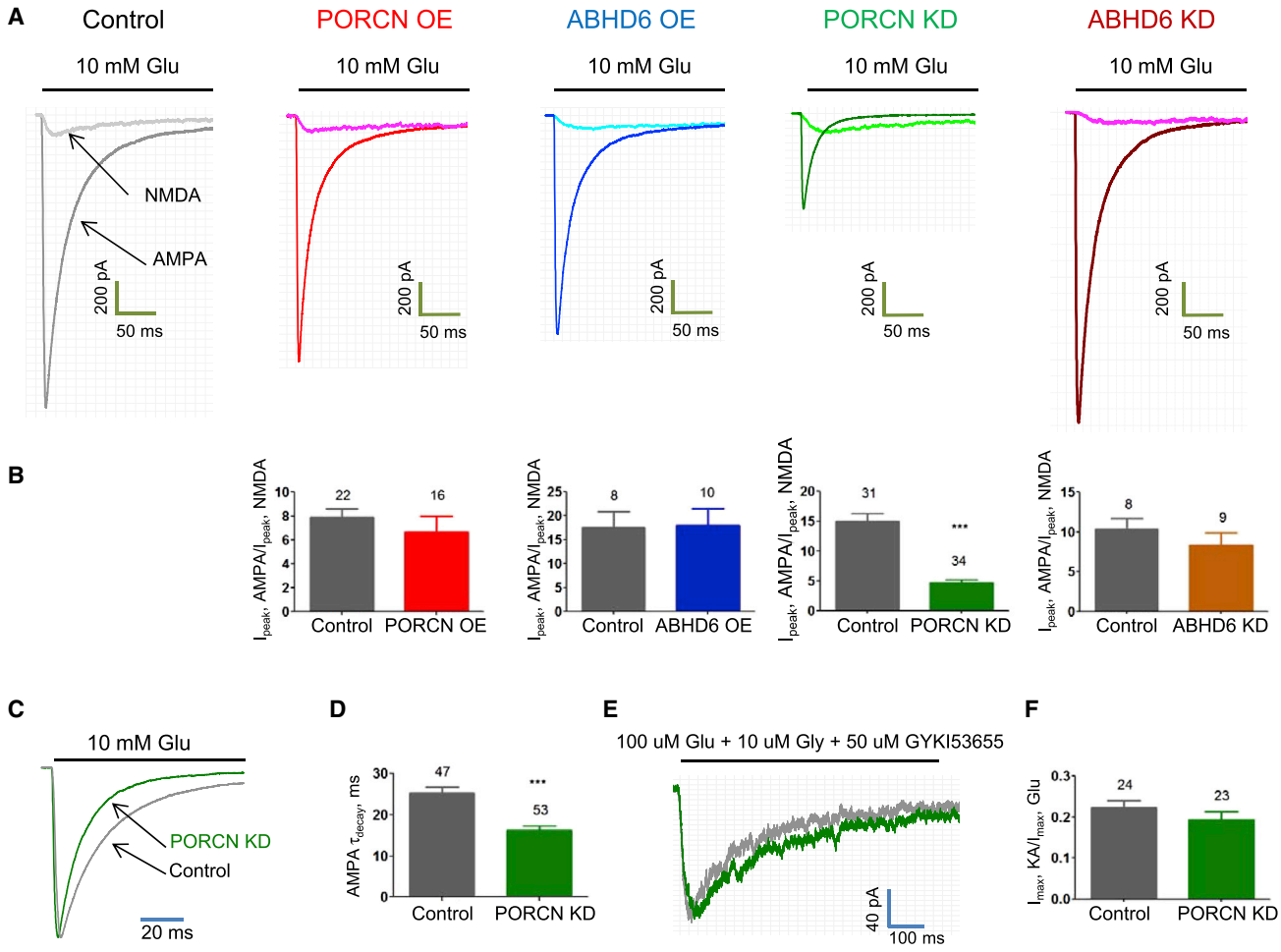

Figure 3. PORCN Knockdown Reduces Glutamate-Evoked Currents and Accelerates Desensitization in Hippocampal Neurons

(A and B) Neither overexpression (OE) of PORCN nor ABHD6 in hippocampal neurons changed glutamate-evoked currents from AMPARs. PORCN knockdown (KD), but not ABHD6 knockdown reduced glutamate-evoked currents in cultured hippocampal neurons. Representative traces of Glu-evoked AMPAR-mediated current and Glu/Gly-evoked NMDA receptor-mediated currents (recorded in the presence of 50 μM GIKY53655) from outside out patches from cultured hippocampal neurons. *$p < 0.05$, **$p < 0.01$, ***$p < 0.001$.

(C–F) Representative normalized glutamate-evoked whole-cell currents (C), weighted tau decay (D), representative NMDA traces overlay (E), and KA to Glu ratio (F) recorded from hippocampal neurons co-transfected with GFP and PORCN shRNA or control.

See also Figures S2 and S3.

AMPAR-mediated currents, PORCN knockdown reduced the average mEPSC amplitude and accelerated the mEPSC decay (Figure 4). The mEPSC frequency also decreased (Figures 4A and 4C). As the shRNA transfection efficiency was <1% (data not shown), the influence of PORCN shRNA on frequency in the GFP-expressing neurons almost certainly reflects postsynaptic effects. This postsynaptic influence on measured frequency likely reflects reduced amplitude leading to miniature events that do not reach threshold. Overexpression of γ-8 in neurons treated with PORCN shRNA failed to rescue the synaptic PORCN knockdown phenotype (Figure 4C).

PORCN Knockdown Selectively Impairs Stability and Composition of Neuronal AMPARs

The reduction in AMPAR-mediated currents with PORCN knockdown is consistent with a model in which PORCN overexpression leads to a disproportionate increase in intracellular GluA1 with decreased surface expression (Figure 1A). Thus, we assessed whether endogenous PORCN stabilizes neuronal AMPAR protein complexes. Hippocampal neurons were infected with lentivirus expressing GFP and PORCN shRNA or GFP and control shRNA and protein lysates were then collected. For these biochemical experiments, high multiplicity of lentivirus infection was used, and >90% of neurons were GFP expressing (data not shown). PORCN knockdown dramatically reduced the amounts of all components of the AMPAR complex evaluated including GluA1, GluA2, γ-8, γ-2, and CNIH-2 (Figure 5A). These effects were specific, as levels of GluK2/3, calnexin, and β-actin were unchanged (Figure 5A). Surface biotinylation showed that PORCN knockdown reduced AMPAR complexes in both intracellular and surface pools (Figure 5A) and strongly suggests that the decreased protein expression underlies the dramatic

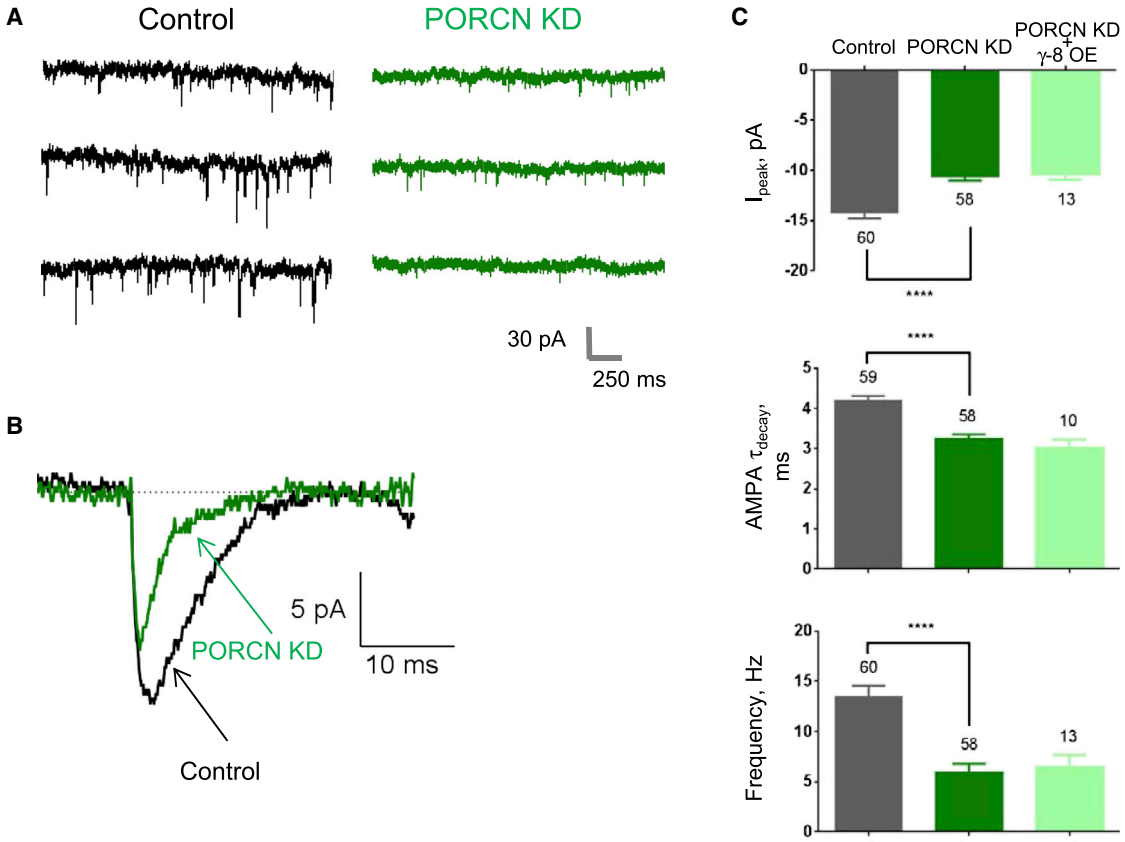

Figure 4. PORCN Knockdown Reduces Hippocampal mEPSCs and Accelerates Their Decay

Hippocampal neurons were co-transfected with GFP and PORCN shRNA or control and mEPSCs were recorded.

(A) Representative traces.

(B) Averaged trace (50 events each) from PORCN-shRNA-transfected or control shRNA-transfected neurons.

(C) Quantification of peak currents, tau decay, and frequency.

reduction in channel function. To visualize this reduction in surface AMPARs, we performed immunofluorescence on hippocampal neurons infected with GFP and either PORCN shRNA or control. This revealed a dramatic reduction in surface GluA1 labeling despite no obvious effects on the dendritic arborization of PORCN shRNA-expressing neurons (Figure 5B).

The acceleration of channel decay kinetics in PORCN knockdown neurons (Figures 3C, 3D, 4B, and 4C) suggests altered composition of the AMPAR complex. One possibility is that PORCN knockdown changes GluA subunit composition such that the more rapidly desensitizing GluA2-lacking receptors become dominant. However, AMPAR channels in PORCN knockdown neurons remain GluA2-containing, as they show typical non-rectifying I/V properties and are not blocked by philanthotoxin (data not shown).

Other possibilities include changes in TARP or CNIH-2 auxiliary subunits, which also slow desensitization (Coombs and Cull-Candy, 2009; Jackson and Nicoll, 2011). To evaluate this, we infected hippocampal neurons with high-titer PORCN shRNA lentivirus. Six days post-infection, we solubilized the neurons, performed AMPAR immunoprecipitations, and immunoblotted for associated and unbound proteins. Immunoprecipitation with a mixture of GluA1–4 antibodies fully bound all AMPAR proteins. Using control cultures, eluates from the GluA1–4 immunoprecipitates contained GluA1, GluA2, γ-8, γ-2, and CNIH-2, whereas β-actin was unbound (Figure 5C). In cultures expressing PORCN shRNA, total levels of all components of the AMPAR complex were decreased (Figure 5C), similar to the results in Figure 5A. In the GluA1–4 immunoprecipitations from PORCN shRNA-expressing neurons, relative partitioning of the remaining γ-2 and CNIH-2 was unaffected, whereas the remaining γ-8 shifted to the unbound fraction (Figure 5C). We repeated this experiment by immunoprecipitating specifically GluA1 from control and PORCN shRNA-treated cultures. Again, we found in PORCN shRNA-expressing cultures that γ-8 was detectable only in the GluA1-unbound fraction, whereas γ-2 remained bound to GluA1 (Figure 5C). Immunoprecipitations from hippocampal lysates performed with either PORCN or TARP γ-8 antibodies demonstrate that there is only a minimal overlapping AMPAR population that contains both PORCN and γ-8 (Figure S4). Together these data suggest that reduced interaction between GluAs and γ-8 may underlie the kinetic effects measured with decreased PORCN expression.

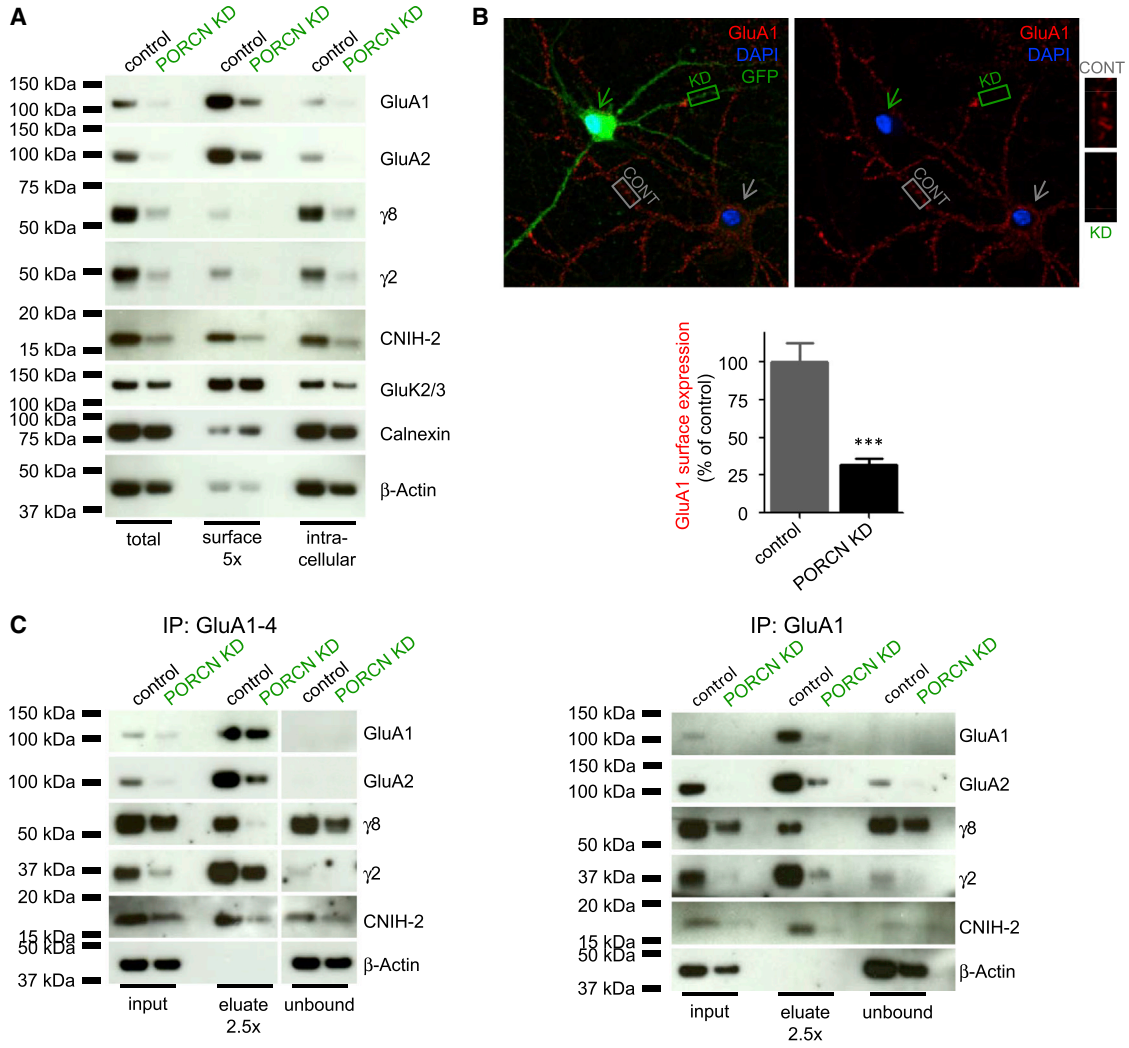

Figure 5. PORCN Knockdown Reduces Levels of AMPAR Components and Dissociates γ-8

(A) Surface biotinylation of hippocampal neurons after infection with PORCN shRNA or control lentivirus. The ER protein calnexin serves as negative control for surface biotinylation, β-actin serves as loading control. PORCN knockdown reduces total and surface levels of AMPAR principal and auxiliary subunits.

(B) Immunolabeling of surface GluA1 in hippocampal neurons DIV 22, 7 days after infection with PORCN shRNA (green arrow) or control (gray arrow) virus. Dendritic regions of infected (green, KD) and non-infected (gray, CONT) neurons are at higher magnification. Quantification of dendritic regions is on the bottom (mean + SEM, n = 18–20, ***$p < 0.001$).

(C) Immunoprecipitation of AMPAR complexes using a mixture of GluA1–4 antibodies (left) or GluA1 antibody alone (right). Following PORCN knockdown, γ-8 is undetectable in AMPAR complexes, whereas γ-2 remains in the complex.

See also Figure S4.

PORCN Knockout Reduces Synaptic and Extrasynaptic AMPAR Complexes

We further assessed the subcellular distribution of PORCN in mouse hippocampus. We found the majority of PORCN accumulated in the P200 fraction, which contains intracellular membranes (Figure 6A). Only a small amount of PORCN was present in the synaptosomal and PSD fractions (Figure 6A) indicating that PORCN is likely shed from AMPARs when the receptors move to the surface.

To investigate further the role of PORCN in brain, we crossed Emx1(Cre) with conditional PORCN knockout mice (Liu et al., 2012) to generate forebrain-specific inducible PORCN knockout mice (PORCN KO), which are viable and without obvious behavioral phenotype though complete PORCN knockout mice die during embryonic development (Barrott et al., 2011). Using hippocampi from these mice, we first conducted a more detailed assessment of the reduced AMPAR complex components measured in Figure 5. Immunoblotting showed that PORCN levels are reduced by about 80% in crude membrane fractions from the KO mice (Figure 6B). Consistent with our previous data, AMPAR components, GluA1, GluA2/3, and γ-8 levels were also reduced in the PORCN KO forebrain, whereas other synaptic proteins, including synaptophysin, PSD-95, and NR1, were unaffected. Similarly, we found selective reduction in

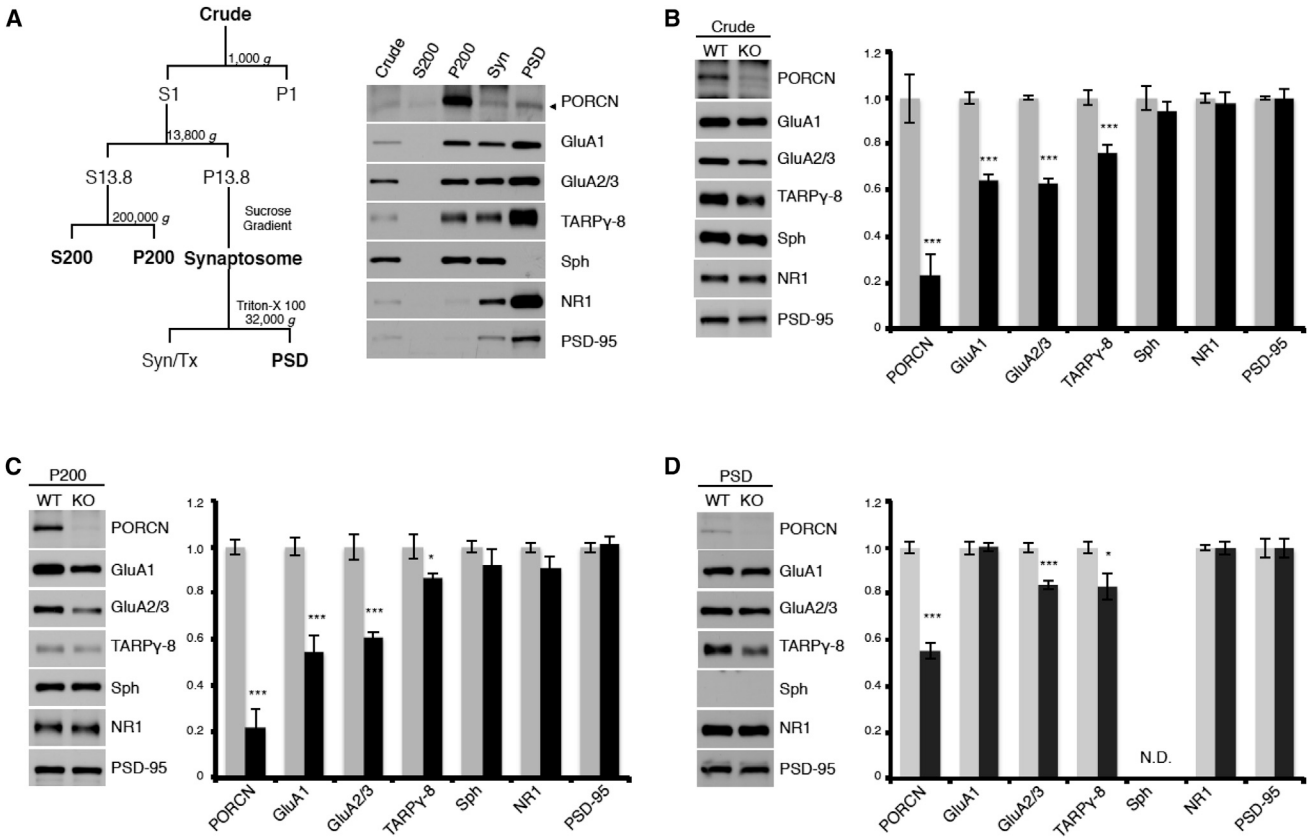

Figure 6. PORCN Fractionates with Intracellular Membranes and Increases AMPAR Levels

(A) Subcellular fractionation of hippocampus shows that PORCN concentrates within intracellular membranes (P200), AMPAR components, and NR1 fractionate with the PSD and synpatophysin occurs in synaptosomes.

(B and C) Quantitative immunoblotting shows that levels of PORCN, GluA1, GluA2/3, and γ-8, but not other synaptic proteins are decreased in both crude extracts (B) and P200 membranes (C) of PORCN KO mice (gray bars, WT; black bars, KO).

(D) GluA2/3 and γ-8 are specifically reduced in the PSD of PORCN KO animals (gray bars, WT; black bars, KO).

See also Figure S5.

components of the AMPAR protein complex in intracellular (P200) membranes from the PORCN KO hippocampus (Figure 6C). In the PSD fraction, GluA2/3 and γ-8 levels were modestly reduced, whereas GluA1 levels were not (Figure 6D).

To investigate further the role for PORCN in stabilizing AMPARs, we treated hippocampal lysates from wild-type and PORCN KO mice with EndoH, which selectively affects AMPA receptors that have not matured from ER through Golgi complex. Interestingly, we found that PORCN KO reduces both the EndoH-sensitive and -resistant GluA2/3 populations proportionately (Figure S5). This differs fundamentally from knockout or overexpression of AMPA receptor auxiliary subunits γ-8 (Rouach et al., 2005) and CNIH-2 (Shi et al., 2010), respectively, which only affect the EndoH-resistant pool of AMPA receptors. These results are consistent with our model that PORCN stabilizes the collective AMPAR pool at the level of the ER.

PORCN Knockout Reduces Basal Synaptic Transmission but Not LTP

We next used acute hippocampal slices from PORCN KO mice to assess basal synaptic function. We recorded extracellular field potentials from stratum radiatum in response to increasing the number of stimulated Schaffer collateral fibers. The slope of the field EPSP (sfEPSP) represents the postsynaptic response and the fiber volley (FV) amplitude provides a measure of the number of active fibers. Consistent with a reduction in AMPAR surface expression, the maximal sfEPSP showed an ~30% reduction in slices from PORCN KO mice ($sfEPSP_{max}$ = 501.5 ± 74.7 and 757.8 ± 119.7 μV/ms in KO and control slices, respectively; n = 13 each, $p < 0.05$, one-way ANOVA with Sidak's multiple comparison test, Figure 7A). In addition, EPSCs from whole-cell recordings of hippocampal CA1 pyramidal cells revealed accelerated decay kinetics in the KO (Figure 7B), which is consistent with results from PORCN shRNA studies in cultured neurons. Evoked synaptic currents from the KOs also had decreased AMPA/NMDA current ratio that fits with the specificity for PORCN in regulating AMPARs (Figure 7C). AMPA/NMDA current ratio in control slices was not changed by a 2 hr incubation with the PORCN inhibitor Wnt-C59 (100 nM), indicating that the effect on AMPA/NMDA ratio is independent of PORCN's enzymatic activity (control: 0.54 ± 0.04, n = 9; Wnt-C59: 0.45 ± 0.07, n = 11; $p > 0.3$). Paired-pulse stimulation showed no

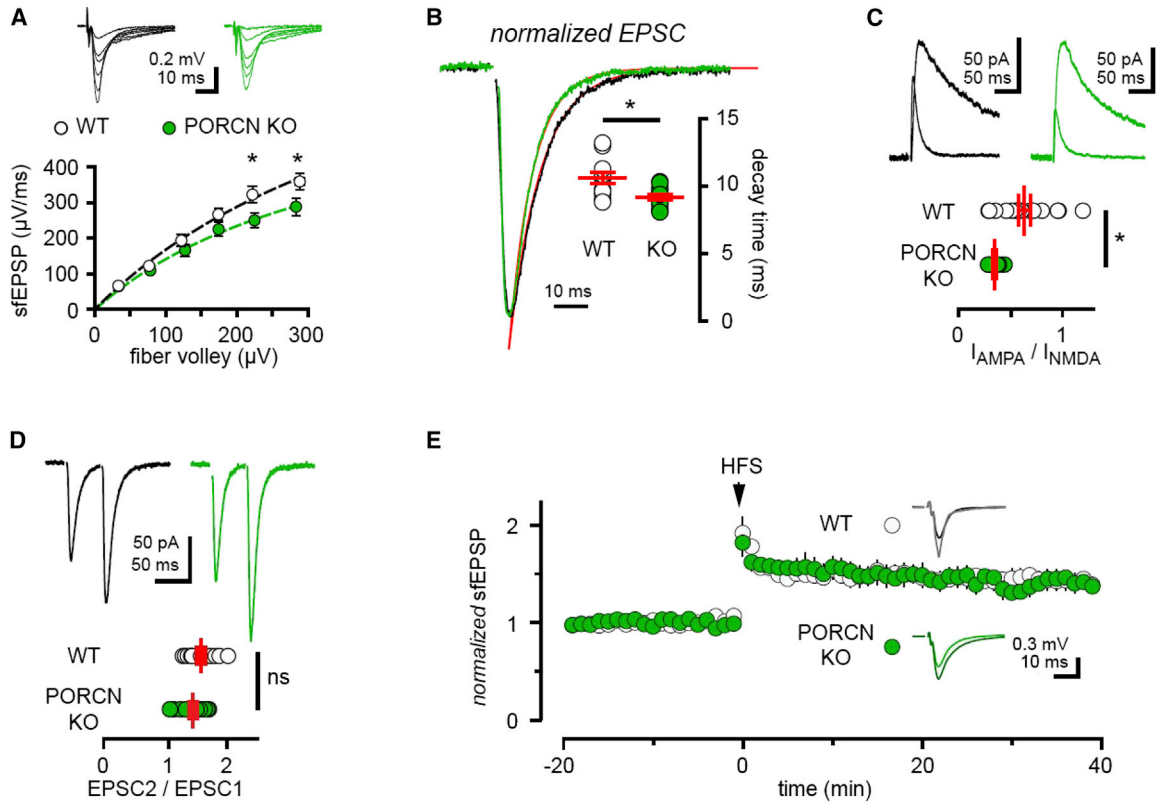

Figure 7. PORCN KO Mice Show Decreased AMPAR-Mediated Transmission and Intact LTP

(A) fEPSP slope plotted against presynaptic fiber volley shows reduced synaptic responses in stratum radiatum of PORCN KO mice. Dotted line denotes least-squares fit of maximal sfEPSP (see Experimental Procedures). WT: n = 23 slices. KO: n = 17 slices, $p < 0.0001$, two-way ANOVA with Sidak's multiple comparison test.

(B) EPSCs in PORCN KO mice show faster decay kinetics compared to WT littermate controls. Superimposed red lines represent least-squares fits of representative traces. (WT: 10.6 ± 0.4 and KO: 9.2 ± 0.2 ms; n = 12 cells each, $p = 0.0065$).

(C) The ratio of AMPA/NMDA current is decreased in PORCN KO mice (WT: 0.64 ± 0.06 and KO: 0.34 ± 0.02, respectively; WT: n = 17 and KO: n = 15 cells. $p = 0.0002$).

(D) Paired-pulse facilitation is not affected by PORCN KO (WT: 1.6 ± 0.07 and KO: 1.4 ± 0.06; n = 12 cells each, $p = 0.1612$).

(E) Slope of extracellular fEPSPs in slices from WT (white) and PORCN KO (green) mice before and after tetanic stimulation (high-frequency stimulation [HFS] at arrow; 2 × 1 s at 100 Hz) of Schaffer collaterals. Inset: averaged representative responses −10 and +30 min HFS (WT: black and gray traces and PORCN KO: green and dark green traces). The magnitude of plasticity was similar in WT and KO slices (35.2% ± 9.4% and 29.8% ± 8.0%, respectively; n = 5 animals each, $p > 0.05$).

difference between PORCN KO and wild-type mice, suggesting that presynaptic function is not altered (Figure 7D). Finally, to assess possible roles for PORCN in regulating synaptic plasticity, we induced LTP using a high-frequency stimulation protocol. As shown in Figure 7E, there was no difference in the normalized fEPSP slope over time between PORCN KO and wild-type animals.

DISCUSSION

This study defines additional functions for PORCN in controlling the stability and the composition of hippocampal AMPARs at the level of the ER. By regulating the number and subunit composition of hippocampal AMPARs, PORCN also controls basal synaptic transmission in vivo. Induction of LTP, however, is independent of PORCN expression. In heterologous cell transfections, in cultured hippocampal neurons and in mouse hippocampus, PORCN expression dramatically increases AMPAR protein levels. In transfected cell lines, PORCN retains AMPARs intracellularly, whereas in neurons PORCN is crucial for maintaining proper assembly and stability of the AMPAR complex and thus, synaptic transmission.

Our focus on PORCN derived from a simple and specific protein stabilization assay coupled with a facile FLIPR assay. That is, we found that three other classes of transmembrane AMPAR-associated proteins, TARPs, CNIH-2, and GSG1-l, all increase GluA1 levels in transfected HEK cells. Using this assay, we surveyed representatives from seven classes of uncharacterized proteins in AMPAR immunoprecipitates and found that both PORCN and ABHD6 increase GluA1 levels. Whereas this stabilization assay may miss some functional interacting proteins, we also performed FLIPR experiments. These studies confirmed that precisely those proteins that increase GluA1 protein levels also modulate GluA1 channel activity. This correlation suggests

Please cite this article in press as: Erlenhardt et al., Porcupine Controls Hippocampal AMPAR Levels, Composition, and Synaptic Transmission, Cell Reports (2016), http://dx.doi.org/10.1016/j.celrep.2015.12.078

utility of the stabilization/FLIPR assay pair, which may enable rapid surveys of other receptor complexes identified by proteomics. As antibodies are not available for all tested protein families, false negative results cannot be excluded.

The stabilizing effect of PORCN on AMPARs also occurs in neurons. Indeed, PORCN knockdown in hippocampal neurons dramatically and specifically decreases levels of all measured components of the AMPAR complex. In parallel, knockout of PORCN in mouse hippocampus results in decreased protein levels of GluA1, GluA2/3, and γ-8. Interestingly, our AMPAR deglycosylation experiments demonstrate that PORCN KO reduces both the EndoH-sensitive and -resistant GluA2/3 populations proportionately, suggesting that PORCN controls the collective AMPAR pool at the level of the ER. This finding is distinct from AMPAR auxiliary subunits like TARPs and CNIHs that preferentially control the EndoH-resistant/mature AMPAR pool (Rouach et al., 2005; Shi et al., 2010). Thus, PORCN is an AMPAR interacting protein that stabilizes the collective AMPAR pool. These findings underscore the unique role of PORCN as an ER chaperone for stabilization and assembly of AMPARs.

In addition to reducing extrasynaptic AMPAR components, PORCN KO also significantly decreases synaptic GluA2/3 and γ-8 levels, which likely explains the reduction in synaptic transmission. Nevertheless, these mutant mice are still competent in LTP induction and maintenance. Our subcellular fractionation and EndoH glycosidase experiments suggest that PORCN stabilizes the collective AMPAR pool at the level of the ER. As PORCN knockout reduces both the surface AMPAR pool and the AMPAR pool for LTP, the mutant mice have proportionate decreases of both basal and potentiated transmission. This results in LTP appearing normal in PORCN KO animals. Similar observations were made in the TARP-γ8-Δ4 knockin mice, which also show reduced synaptic transmission, but no changes in LTP (Sumioka et al., 2011). In contrast, knockout of PSD-95 decreases synaptic transmission and increases LTP (Migaud et al., 1998), as PSD-95 anchors synaptic AMPARs but does not regulate the AMPAR pool for LTP. On the other hand, CaMKII is important for induction of LTP but does not control the number of synaptic AMPARs under basal conditions. Accordingly, CaMKII mutant mice show normal basal transmission but decreased LTP (Silva et al., 1992).

Besides the described changes in protein expression and thus in current amplitudes, deletion of PORCN also leads to accelerated decay kinetics of evoked and spontaneous AMPAR currents. These changes in channel kinetics are most likely a secondary effect due to the selective depletion of γ-8 but not γ-2 from AMPAR complexes in the absence of PORCN, as γ-8 has greater effects on AMPAR desensitization (Cho et al., 2007; Milstein et al., 2007). However, decay kinetics could not be rescued by overexpression of γ-8. Changes in the synaptic current decay kinetics could also be explained by the selective reduction of GluA2/3 protein levels in the PSD fraction of PORCN KO mice, leaving faster desensitizing GluA2-lacking receptors at the synapse. Experiments in dissociated neuronal cultures, however, did not show significant changes in rectification properties or block by philanthotoxin demonstrating that most neuronal AMPARs are still GluA2 containing. A direct effect of PORCN on AMPAR kinetics is alternatively possible, but unlikely as PORCN levels in the PSD are minimal.

Both ABHD6 and PORCN have transmembrane domains, and both have well-characterized enzyme activities. ABHD6 serves as the rate-limiting enzyme in degrading the endocannabinoid 2-AG and localizes postsynaptically (Marrs et al., 2010). Knockdown of ABHD6 or pharmacological inhibition augments endocannabinoid signaling and thereby modulates synaptic plasticity (Zhong et al., 2011). However, these properties are not essential for actions described here, as a catalytically inactive ABHD6 mutant (Navia-Paldanius et al., 2012) continued to modulate AMPARs.

Porcupine was discovered genetically as acting upstream of the segment polarity gene *wingless* (*Wg*), a *Drosophila* Wnt family member (Kadowaki et al., 1996). Elegant genetic and biochemical studies later showed that PORCN mediates palmitoylation of a specific serine on Wg and mammalian Wnt isoforms (Galli et al., 2007). These Wg/Wnt palmitoylations occur in the lumen of the ER and are therefore categorically distinct from cytoplasmic palmitoylations catalyzed by DHHC enzymes that modify the C-terminal tail of AMPARs, PSD-95, and many other synaptic proteins (El-Husseini and Bredt, 2002; Hayashi et al., 2005).

Palmitoyl-transferase activity of PORCN does not mediate its effects on AMPARs, as a catalytically dead mutant (Galli et al., 2007) showed full activity to control GluA1 stability. Additionally, a highly specific and potent PORCN inhibitor did not abolish the PORCN-mediated effects on AMPARs in HEK cells or neurons. Importantly, recent genetic studies found that PORCN effects on a subset of cancer cell lines are independent of its enzyme activity. Indeed, PORCN mutated at the same His used here was fully effective in controlling cell growth in multiple breast cancer cell lines (Covey et al., 2012). Thus, PORCN's functional interaction with AMPARs occurs in a "moonlighting" role independent of Wnt signaling. Another multi-functional ion channel modulator is gephyrin, which both clusters glycine/GABA receptors in neurons and catalyzes the last step in molybdenum cofactor biosynthesis throughout the body (Feng et al., 1998). Like gephyrin, PORCN is a single gene subject to complex alternative splicing. It will be important to understand how these alternative forms may specify PORCN actions on Wnt and non-Wnt pathways.

PORCN has differential effects on AMPARs in heterologous cells and neurons. Whereas PORCN expression dramatically increases levels of AMPARs in both systems, PORCN reduces receptor functionality in non-neuronal cells. This reduced functionality is due to PORCN-dependent retention of GluA subunits in intracellular compartments as demonstrated by biotinylation experiments, and it is not due to an increased cytoplasmic polyamine block as shown by rectification experiments (data not shown). As AMPARs are expressed almost exclusively in neurons and glial cells, this intracellular trapping in HEK293T cells may be artificial. Alternatively, PORCN may physiologically retain GluA subunits in the ER and release them following proper assembly of the AMPAR complex. Co-expression of TARPs did not overcome PORCN-mediated intracellular retention of GluA1 (data not shown), so other neuronal factors or other AMPAR auxiliary subunits must contribute. Cellular context is also critical in function of CNIH-2, which promotes ER export of AMPARs in mammalian neurons (Harmel et al., 2012) but reduces AMPAR surface levels in oocytes (Brockie et al., 2013).

Furthermore, in *C. elegans* muscle cells, CNIH-2 or its worm homolog CNI-1 blocks ER export and CNIH-2 reduces surface AMPAR levels (Brockie et al., 2013).

The expanding catalog of glutamate receptor auxiliary subunits and associated transmembrane proteins underscores the importance and complexity of the receptor complexes. Whereas the interactions described here specifically control AMPARs, distinct auxiliary subunits, Neto-1/2, modulate neuronal kainate receptors (Tomita and Castillo, 2012). The evolutionary conservation of these interacting proteins emphasizes that they serve fundamental roles (Wang et al., 2008). In *C. elegans*, the mixed AMPA/kainate receptor GLR-1 associates with STG (TARP-like), CNI (CNIH-2-like), and SOL (NETO-like). Elegant genetic studies in *C. elegans* have defined how these subunits globally regulate glutamate receptor number and function at worm synapses (Brockie et al., 2013). Analogous studies of the larger mammalian AMPAR complex represent a major challenge.

Selective enrichment of PORCN in principal cells in hippocampus fits with its role in controlling incorporation of γ-8, which also has highest expression in these neurons. Similarly, CNIH-2 is concentrated in hippocampal neurons, where it specifically controls γ-8-containing AMPAR complexes (Herring et al., 2013; Kato et al., 2010). As hippocampal neurons play especially important roles in spatial navigation and memory consolidation, they may require multiple and complex mechanisms for controlling AMPAR trafficking and gating. Defining how this molecular ensemble orchestrates development and plasticity of hippocampal synapses will provide insights for understanding memory formation and how it goes awry in neuropsychiatric disorders.

EXPERIMENTAL PROCEDURES

FLIPR Assay

HEK293T cells were seeded into poly-D-lysine-coated, clear-bottom black 96-well plates (BD Biosciences) at a density of 50,000 cells/well. Forty-eight hours after transfection with Fugene HD (Promega), cells were washed three times in assay buffer (in mM: 137 NaCl, 4 KCl, 2 $CaCl_2$, 1 $MgCl_2$, 10 HEPES, 5 D-Glucose [pH 7.4]). Cells were incubated with 1 × FLIPR Calcium 5 Assay Kit (Molecular Devices) in assay buffer supplemented with 1.25 mM probenicid for 1 hr. After washing the cells, plates were transferred to the FLIPR Tetra System (Molecular Devices). Glutamate responses (100 μM) were calculated as max–min between 8 and 160 s. Experiments were run as triplicates or quadruplicates on each plate.

Quantification of GluA Surface Expression in HEK Cells and Cultured Hippocampal Neurons

Surface expression of extracellularly hemagglutinin-tagged (HA-tagged) GluA1 was performed as described previously (Harmel et al., 2012). In brief, cells were fixed in 4% paraformaldehyde, blocked with 10% normal goat serum in PBS, followed by incubation with an anti-HA antibody (1:100, Santa Cruz Biotechnology) and a secondary goat-anti-mouse-HRP antibody (1:10,000, Santa Cruz). Chemiluminescence was quantified in a GloMax 20/20 luminometer (Promega) using SuperSignal ELISA Femto Maximum Sensitivity Substrate (Pierce). Surface expression of extracellularly stained AMPARs in cultured hippocampal neurons was quantified by fluorescence intensity measurements of anti-GluA1 immunocytochemistry without use of detergents. Hippocampal neurons were incubated with primary antibody (1:100, mouse anti-GluA1-NT, Millipore) in culture medium for 30 min at 37°C. Cells were washed three times with ice-cold PBS and fixed with 4% paraformaldehyde in PBS for 10 min at 4°C. Cells were blocked for 30 min in 10% normal goat serum in PBS before incubation with an Alexa Fluor 555-conjugated goat-anti-mouse antibody (1:500 in 10% normal goat serum in PBS, Molecular Probes) for 30 min at room temperature. To identify dendrites, cells were permeabilized with 0.04% Triton X-100 in PBS and stained with a chicken anti-MAP2 antibody (1:1,000, Millipore) and a secondary goat-anti-chicken antibody conjugated to Alexa Fluor 647 (Molecular Probes). Nuclei were stained using the NucBlue Fixed Cell Stain DAPI (Molecular Probes). Neurons were mounted and imaged using a confocal LSM710 from Zeiss. Test and control groups were processed in parallel. Mean intensity values of surface staining were measured after background correction for 18–20 different secondary dendrites from four different coverslips. Data were quantified using ImageJ software (NIH).

Immunoprecipitation

Crude membrane fractions of cultured hippocampal neurons were solubilized in ComplexioLyte buffer CL-91 (Logopharm GmbH) for 30 min on ice and incubated with immobilized antibodies for 2 hr at 4°C. The following mixture of antibodies was used: 30% of anti-GluA1 (AB1504, Millipore), 35% of anti-GluA2 (AB1768, Millipore), 25% of anti-GluA2/3 (07-598, Millipore), and 10% of anti-GluA4 (AB1508, Millipore). After brief washing with 0.1% CL-91, bound proteins were eluted with 50 mM glycine (pH 2.8) for 10 min at 37°C. Bolt LDS Sample Buffer and Bolt Sample Reducing Agent (Life Technologies) were added before denaturation at 37°C for 10 min.

Electrophysiology in HEK293T Cells and Cultured Primary Neurons

Agonist-evoked currents were recorded from transfected HEK293T cells or outside out patches from cultured primary hippocampal neurons. Recordings were made using thick-walled boroscillicate glass electrodes pulled to a resistance of 2–5 MΩ. All cells were voltage-clamped at −60 mV, and data were collected and digitized using an Axopatch 200B and Clampex 9.2 software (Molecular Devices). For whole-cell recordings, the transfected HEK293T cells were bathed in external solution containing (in mM): 137 NaCl, 4 KCl, 2 $CaCl_2$, 1 $MgCl_2$, 5 glucose, and 10 Na-HEPES (pH 7.4), ~300 mOsm. For cultured primary neurons, 10 μM CPP, 10 μM bicuculline, and 0.3 μM TTX were added to the external solution. The intracellular electrode solution contained (in mM): 90 KF, 30 KCl, 5 EGTA, and 10 Na-HEPES (pH 7.4), ~290 mOsm. Data were acquired at 20 kHz and filtered at 2 kHz. Whole-cell responses were measured by rapidly transitioning to the external solution containing agonist for 500 ms using glass perfusion barrels driven by a SF-77B Perfusion Fast-Step (Warner Instruments). Agonist-evoked currents were quantified using Clampfit software (Molecular Devices) to calculate the mean current amplitude using the last five sweeps after the agonist response was stable.

Spontaneous AMPAR-mediated miniature excitatory post-synaptic currents (mEPSC) from hippocampal neurons (days in vitro [DIV] 20–26) were recorded in the presence of 10 μM bicuculline, 10 μM CPP, 300 nM TTX, in whole-cell configuration at a holding potential of −60 mV. Typically, 50 consecutive events of mEPSCs were used for analysis. They were inspected visually and were selected with a lower limit amplitude cutoff of greater than 10 pA. Amplitude and frequency of events were analyzed using Minianalysis (Synaptosoft). mEPSCs were fitted with bi-exponential functions to determine decay kinetics (weighted tau).

Electrophysiology and Chemiluminescence Assay Using *Xenopus laevis* Oocytes

Two electrode voltage clamp recordings and chemiluminescence assay of surface proteins were performed as described (Morimoto-Tomita et al., 2009). In brief, cRNAs were injected into *Xenopus laevis* oocytes and defolliculated, and experiments were performed at 4–5 days after injection. Two-electrode voltage-clamp analysis (V_h = −70 mV) was done at room temperature. Glutamate was bath applied in recording solution (90 mM NaCl, 1.0 mM KCl, 1.5 mM $CaCl_2$, and 10 mM HEPES [pH 7.4]). For surface labeling, oocytes were incubated with rat anti-HA antibody (3F10, Roche) followed by incubation with HRP-conjugated anti-rat Ig. Chemiluminescence was quantified with SuperSignal ELISA Femto Maximum Sensitivity Substrate (Pierce).

Slice Electrophysiology

Schaeffer collaterals were stimulated at 0.1 Hz with a bipolar nickel-chromate wire electrode. The fiber volley and EPSP (fEPSP) were recorded from stratum radiatum using 1–2 MΩ pipettes filled with ACSF. fEPSPs were quantified by

Please cite this article in press as: Erlenhardt et al., Porcupine Controls Hippocampal AMPAR Levels, Composition, and Synaptic Transmission, Cell Reports (2016), http://dx.doi.org/10.1016/j.celrep.2015.12.078

measuring the initial slope (by linear regression sfEPSP) following the fiber volley (FV). Each input-output curve was fitted with the equation.

$sfEPSP_{FV}(i) = sfEPSP_{max} \times FV^h \div (sfEPSP_{50}^h + FV^h)$ where $sfEPSP_{FV}(i)$ is the sfEPSP with fiber volley amplitude FV, $sfEPSP_{50}$ is the sfEPSP yielding the half maximal response, $sfEPSP_{max}$ is the maximal sfEPSP, and h is the slope of the input-output curve. Whole-cell voltage clamp recordings from CA1 pyramidal neurons were made using 2- to 4-MΩ pipettes filled with intracellular solution containing (in mM) 135 $CsMeSO_3$, 10 CsCl, 10 HEPES, 1 EGTA, 4 MgATP, 0.4 NaGTP, and extracellular ACSF with the addition of picrotoxin (100 μM) and (R)-CPP (100 μM; Tocris Bioscience) unless otherwise specified. To minimize epileptiform activity, a cut was made between CA1 and CA3. Data were collected using Multiclamp 700B amplifier, filtered at 2–4 KHz, and digitized at 10–50 kHz (Digidata 1440, Molecular Devices).

Paired-pulse stimulation (50-ms inter-stimulus interval) was assessed at −60 mV. AMPAR/NMDAR ratio was determined by first recording EPSCs at +40 mV followed by AMPAR currents in the presence of (R)-CPP. NMDAR currents were then obtained by digital off-line subtraction of AMPAR current.

LTP experiments were performed in coronal sections bathed in ACSF (2.5 mM Ca^{2+}/ 1.3 mM Mg^{2+}) warmed to 28°C. A stable 20-min baseline of fEPSPs in response to half-maximal stimulation was obtained followed by LTP induction using a high-frequency protocol: 100 Hz train for 1 s, delivered twice, 20 s apart.

Data were analyzed using AxoGraphX software and displayed as means ± SEM. Significance was analyzed either with two-tailed Student's t tests or a one- or two-way ANOVAs with a Sidak's multiple comparison test (Microsoft Excel and GraphPad Prism). n values indicate number of cells or slices.

SUPPLEMENTAL INFORMATION

Supplemental Information includes Supplemental Experimental Procedures and five figures and can be found with this article online at http://dx.doi.org/10.1016/j.celrep.2015.12.078.

AUTHOR CONTRIBUTIONS

D.S.B., N.E., H.Y., S.T., and J.I.W. designed research. N.E., H.Y., K.A., and T.Y. performed experiments and analyzed data. D.S.B. and N.E. wrote the paper.

ACKNOWLEDGMENTS

This work is partially supported by NIH/NIMH MH085080 (S.T.) and NIH/NINDS NS065920 (J.I.W.). We thank the McMahon lab (UAB) for help and advice with the plasticity experiments. We thank Dr. Ignatia B. Van den Veyver (Baylor College of Medicine), Dr. Kevin R. Jones (University of Colorado-Boulder), and Jackson Laboratory for generating and maintaining conditional PORCN and Emx1(Cre) mice. Requests for PORCN KO mice should be addressed to susumu.tomita@yale.edu

Received: February 6, 2014
Revised: November 19, 2015
Accepted: December 15, 2015
Published: January 14, 2016

REFERENCES

Anggono, V., and Huganir, R.L. (2012). Regulation of AMPA receptor trafficking and synaptic plasticity. Curr. Opin. Neurobiol. *22*, 461–469.

Barrott, J.J., Cash, G.M., Smith, A.P., Barrow, J.R., and Murtaugh, L.C. (2011). Deletion of mouse Porcn blocks Wnt ligand secretion and reveals an ectodermal etiology of human focal dermal hypoplasia/Goltz syndrome. Proc. Natl. Acad. Sci. USA *108*, 12752–12757.

Bats, C., Farrant, M., and Cull-Candy, S.G. (2013). A role of TARPs in the expression and plasticity of calcium-permeable AMPARs: evidence from cerebellar neurons and glia. Neuropharmacology *74*, 76–85.

Boulter, J., Hollmann, M., O'Shea-Greenfield, A., Hartley, M., Deneris, E., Maron, C., and Heinemann, S. (1990). Molecular cloning and functional expression of glutamate receptor subunit genes. Science *249*, 1033–1037.

Brockie, P.J., Jensen, M., Mellem, J.E., Jensen, E., Yamasaki, T., Wang, R., Maxfield, D., Thacker, C., Hoerndli, F., Dunn, P.J., et al. (2013). Cornichons control ER export of AMPA receptors to regulate synaptic excitability. Neuron *80*, 129–142.

Cho, C.H., St-Gelais, F., Zhang, W., Tomita, S., and Howe, J.R. (2007). Two families of TARP isoforms that have distinct effects on the kinetic properties of AMPA receptors and synaptic currents. Neuron *55*, 890–904.

Coombs, I.D., and Cull-Candy, S.G. (2009). Transmembrane AMPA receptor regulatory proteins and AMPA receptor function in the cerebellum. Neuroscience *162*, 656–665.

Covey, T.M., Kaur, S., Tan Ong, T., Proffitt, K.D., Wu, Y., Tan, P., and Virshup, D.M. (2012). PORCN moonlights in a Wnt-independent pathway that regulates cancer cell proliferation. PLoS ONE *7*, e34532.

Ehlers, M.D. (2000). Reinsertion or degradation of AMPA receptors determined by activity-dependent endocytic sorting. Neuron *28*, 511–525.

El-Husseini, Ael.-D., and Bredt, D.S. (2002). Protein palmitoylation: a regulator of neuronal development and function. Nat. Rev. Neurosci. *3*, 791–802.

Feng, G., Tintrup, H., Kirsch, J., Nichol, M.C., Kuhse, J., Betz, H., and Sanes, J.R. (1998). Dual requirement for gephyrin in glycine receptor clustering and molybdoenzyme activity. Science *282*, 1321–1324.

Galli, L.M., Barnes, T.L., Secrest, S.S., Kadowaki, T., and Burrus, L.W. (2007). Porcupine-mediated lipid-modification regulates the activity and distribution of Wnt proteins in the chick neural tube. Development *134*, 3339–3348.

Harmel, N., Cokic, B., Zolles, G., Berkefeld, H., Mauric, V., Fakler, B., Stein, V., and Klöcker, N. (2012). AMPA receptors commandeer an ancient cargo exporter for use as an auxiliary subunit for signaling. PLoS ONE *7*, e30681.

Hashimoto, K., Fukaya, M., Qiao, X., Sakimura, K., Watanabe, M., and Kano, M. (1999). Impairment of AMPA receptor function in cerebellar granule cells of ataxic mutant mouse stargazer. J. Neurosci. *19*, 6027–6036.

Hayashi, T., Rumbaugh, G., and Huganir, R.L. (2005). Differential regulation of AMPA receptor subunit trafficking by palmitoylation of two distinct sites. Neuron *47*, 709–723.

Herring, B.E., Shi, Y., Suh, Y.H., Zheng, C.Y., Blankenship, S.M., Roche, K.W., and Nicoll, R.A. (2013). Cornichon proteins determine the subunit composition of synaptic AMPA receptors. Neuron *77*, 1083–1096.

Huganir, R.L., and Nicoll, R.A. (2013). AMPARs and synaptic plasticity: the last 25 years. Neuron *80*, 704–717.

Jackson, A.C., and Nicoll, R.A. (2011). The expanding social network of ionotropic glutamate receptors: TARPs and other transmembrane auxiliary subunits. Neuron *70*, 178–199.

Kadowaki, T., Wilder, E., Klingensmith, J., Zachary, K., and Perrimon, N. (1996). The segment polarity gene porcupine encodes a putative multitransmembrane protein involved in Wingless processing. Genes Dev. *10*, 3116–3128.

Kato, A.S., and Bredt, D.S. (2007). Pharmacological regulation of ion channels by auxiliary subunits. Curr. Opin. Drug Discov. Devel. *10*, 565–572.

Kato, A.S., Gill, M.B., Ho, M.T., Yu, H., Tu, Y., Siuda, E.R., Wang, H., Qian, Y.-W., Nisenbaum, E.S., Tomita, S., and Bredt, D.S. (2010). Hippocampal AMPA receptor gating controlled by both TARP and cornichon proteins. Neuron *68*, 1082–1096.

Lein, E.S., Hawrylycz, M.J., Ao, N., Ayres, M., Bensinger, A., Bernard, A., Boe, A.F., Boguski, M.S., Brockway, K.S., Byrnes, E.J., et al. (2007). Genome-wide atlas of gene expression in the adult mouse brain. Nature *445*, 168–176.

Liu, W., Shaver, T.M., Balasa, A., Ljungberg, M.C., Wang, X., Wen, S., Nguyen, H., and Van den Veyver, I.B. (2012). Deletion of Porcn in mice leads to multiple developmental defects and models human focal dermal hypoplasia (Goltz syndrome). PLoS ONE *7*, e32331.

Lum, L., and Clevers, H. (2012). Cell biology. The unusual case of Porcupine. Science *337*, 922–923.

Malinow, R., and Malenka, R.C. (2002). AMPA receptor trafficking and synaptic plasticity. Annu. Rev. Neurosci. *25*, 103–126.

Marrs, W.R., Blankman, J.L., Horne, E.A., Thomazeau, A., Lin, Y.H., Coy, J., Bodor, A.L., Muccioli, G.G., Hu, S.S., Woodruff, G., et al. (2010). The serine hydrolase ABHD6 controls the accumulation and efficacy of 2-AG at cannabinoid receptors. Nat. Neurosci. *13*, 951–957.

Migaud, M., Charlesworth, P., Dempster, M., Webster, L.C., Watabe, A.M., Makhinson, M., He, Y., Ramsay, M.F., Morris, R.G., Morrison, J.H., et al. (1998). Enhanced long-term potentiation and impaired learning in mice with mutant postsynaptic density-95 protein. Nature *396*, 433–439.

Milstein, A.D., Zhou, W., Karimzadegan, S., Bredt, D.S., and Nicoll, R.A. (2007). TARP subtypes differentially and dose-dependently control synaptic AMPA receptor gating. Neuron *55*, 905–918.

Morimoto-Tomita, M., Zhang, W., Straub, C., Cho, C.H., Kim, K.S., Howe, J.R., and Tomita, S. (2009). Autoinactivation of neuronal AMPA receptors via glutamate-regulated TARP interaction. Neuron *61*, 101–112.

Navia-Paldanius, D., Savinainen, J.R., and Laitinen, J.T. (2012). Biochemical and pharmacological characterization of human α/β-hydrolase domain containing 6 (ABHD6) and 12 (ABHD12). J. Lipid Res. *53*, 2413–2424.

Nicoll, R.A., Tomita, S., and Bredt, D.S. (2006). Auxiliary subunits assist AMPA-type glutamate receptors. Science *311*, 1253–1256.

Proffitt, K.D., Madan, B., Ke, Z., Pendharkar, V., Ding, L., Lee, M.A., Hannoush, R.N., and Virshup, D.M. (2013). Pharmacological inhibition of the Wnt acyltransferase PORCN prevents growth of WNT-driven mammary cancer. Cancer Res. *73*, 502–507.

Rouach, N., Byrd, K., Petralia, R.S., Elias, G.M., Adesnik, H., Tomita, S., Karimzadegan, S., Kealey, C., Bredt, D.S., and Nicoll, R.A. (2005). TARP gamma-8 controls hippocampal AMPA receptor number, distribution and synaptic plasticity. Nat. Neurosci. *8*, 1525–1533.

Schwenk, J., Harmel, N., Zolles, G., Bildl, W., Kulik, A., Heimrich, B., Chisaka, O., Jonas, P., Schulte, U., Fakler, B., and Klöcker, N. (2009). Functional proteomics identify cornichon proteins as auxiliary subunits of AMPA receptors. Science *323*, 1313–1319.

Schwenk, J., Harmel, N., Brechet, A., Zolles, G., Berkefeld, H., Müller, C.S., Bildl, W., Baehrens, D., Hüber, B., Kulik, A., et al. (2012). High-resolution proteomics unravel architecture and molecular diversity of native AMPA receptor complexes. Neuron *74*, 621–633.

Seeburg, P.H. (1993). The TINS/TiPS Lecture. The molecular biology of mammalian glutamate receptor channels. Trends Neurosci. *16*, 359–365.

Shanks, N.F., Savas, J.N., Maruo, T., Cais, O., Hirao, A., Oe, S., Ghosh, A., Noda, Y., Greger, I.H., Yates, J.R., 3rd, and Nakagawa, T. (2012). Differences in AMPA and kainate receptor interactomes facilitate identification of AMPA receptor auxiliary subunit GSG1L. Cell Rep. *1*, 590–598.

Sheng, M., and Kim, M.J. (2002). Postsynaptic signaling and plasticity mechanisms. Science *298*, 776–780.

Shi, Y., Lu, W., Milstein, A.D., and Nicoll, R.A. (2009). The stoichiometry of AMPA receptors and TARPs varies by neuronal cell type. Neuron *62*, 633–640.

Shi, Y., Suh, Y.H., Milstein, A.D., Isozaki, K., Schmid, S.M., Roche, K.W., and Nicoll, R.A. (2010). Functional comparison of the effects of TARPs and cornichons on AMPA receptor trafficking and gating. Proc. Natl. Acad. Sci. USA *107*, 16315–16319.

Silva, A.J., Paylor, R., Wehner, J.M., and Tonegawa, S. (1992). Impaired spatial learning in alpha-calcium-calmodulin kinase II mutant mice. Science *257*, 206–211.

Straub, C., and Tomita, S. (2012). The regulation of glutamate receptor trafficking and function by TARPs and other transmembrane auxiliary subunits. Curr. Opin. Neurobiol. *22*, 488–495.

Sumioka, A., Brown, T.E., Kato, A.S., Bredt, D.S., Kauer, J.A., and Tomita, S. (2011). PDZ binding of TARPγ-8 controls synaptic transmission but not synaptic plasticity. Nat. Neurosci. *14*, 1410–1412.

Tomita, S., and Castillo, P.E. (2012). Neto1 and Neto2: auxiliary subunits that determine key properties of native kainate receptors. J. Physiol. *590*, 2217–2223.

Tomita, S., Chen, L., Kawasaki, Y., Petralia, R.S., Wenthold, R.J., Nicoll, R.A., and Bredt, D.S. (2003). Functional studies and distribution define a family of transmembrane AMPA receptor regulatory proteins. J. Cell Biol. *161*, 805–816.

Tomita, S., Adesnik, H., Sekiguchi, M., Zhang, W., Wada, K., Howe, J.R., Nicoll, R.A., and Bredt, D.S. (2005). Stargazin modulates AMPA receptor gating and trafficking by distinct domains. Nature *435*, 1052–1058.

Tomita, S., Byrd, R.K., Rouach, N., Bellone, C., Venegas, A., O'Brien, J.L., Kim, K.S., Olsen, O., Nicoll, R.A., and Bredt, D.S. (2007). AMPA receptors and stargazin-like transmembrane AMPA receptor-regulatory proteins mediate hippocampal kainate neurotoxicity. Proc. Natl. Acad. Sci. USA *104*, 18784–18788.

von Engelhardt, J., Mack, V., Sprengel, R., Kavenstock, N., Li, K.W., Stern-Bach, Y., Smit, A.B., Seeburg, P.H., and Monyer, H. (2010). CKAMP44: a brain-specific protein attenuating short-term synaptic plasticity in the dentate gyrus. Science *327*, 1518–1522.

Wang, R., Walker, C.S., Brockie, P.J., Francis, M.M., Mellem, J.E., Madsen, D.M., and Maricq, A.V. (2008). Evolutionary conserved role for TARPs in the gating of glutamate receptors and tuning of synaptic function. Neuron *59*, 997–1008.

Yan, D., and Tomita, S. (2012). Defined criteria for auxiliary subunits of glutamate receptors. J. Physiol. *590*, 21–31.

Zhang, W., St-Gelais, F., Grabner, C.P., Trinidad, J.C., Sumioka, A., Morimoto-Tomita, M., Kim, K.S., Straub, C., Burlingame, A.L., Howe, J.R., and Tomita, S. (2009). A transmembrane accessory subunit that modulates kainate-type glutamate receptors. Neuron *61*, 385–396.

Zhong, P., Pan, B., Gao, X.P., Blankman, J.L., Cravatt, B.F., and Liu, Q.S. (2011). Genetic deletion of monoacylglycerol lipase alters endocannabinoid-mediated retrograde synaptic depression in the cerebellum. J. Physiol. *589*, 4847–4855.